

NUMERICAL SIMULATION OF TORNADOES GENERATED BY A TYPHOON NEAR A COASTAL LINE

Ken-ichi Shimose* and Tetsuya Kawano

Department of Earth and Planetary Sciences, Kyushu University, Fukuoka, Japan

1. INTRODUCTION

Tropical cyclones (hereafter, TC) as typhoons or hurricanes frequently spawn tornadoes. McCaul (1991) reported that approximately 59% of hurricanes that hit the United States during the period of 1948-86 produced at least one tornado. Most of the reported tornadoes are produced within two areas of TCs: near the core of the storm and in the outer rainbands (Gentry 1983). McCaul (1991) noted that shear and helicity are most favorable for tornadoes in the right-front quadrant. Nearly all hurricane-induced tornadoes occur on land within 200 km of the coast (Nolvan and Gray 1974), because surface wind speeds over land areas were reduced by friction while the flow at slightly higher levels remained strong and was not affected by friction (Gentry 1983). Spratt et al. (1997) used the observation by the WSR-88D and revealed that many of the tornadoes are related to intense, persistent cells within the outer rainbands. McCaul and Weisman (1996) simulated shallow supercell storms in landfalling hurricane environments and found that the storm's updrafts were produced by the strong upward dynamic pressure gradient force and relatively weak buoyancy and the vertical vorticity of the mesocyclone was generated by tilting and stretching of the horizontal vorticity, which was generated by the strong vertical shear. TC-spawned tornadoes, however, have not understood completely because of the lack of three-dimensional data such as multiple Doppler radars observations. It is important for the comprehension of TC-spawned tornadoes to obtain high-resolution three-dimensional data by multiple Doppler radars or realistic numerical simulations.

In this study, we describe a case study of tornadoes generated by Typhoon 0613 (T0613) in the coastal region of the Miyazaki Plain (see Fig.1), the southwestern part of Japan on 17 September 2006. In the region, typhoon-spawned tornadoes frequently occurred; from 1971 to 2006, there were twenty-three tornadoes and fifteen of them (approximately 65%) associated with typhoons. Almost all tornadoes occurred in the right-front

quadrant of the typhoons. Saito (1992) analyzed tornadoes associated with Typhoon 8019 in 1980 in the Miyazaki Plain and found that the tornadoes were accompanied by mesocyclones in the parent storms. However, there is no Doppler radar in this region so that it is difficult to understand the tornadogenesis by using the observation data. Thus, we attempt to investigate the tornadoes associated with the typhoon using high-resolution realistic numerical simulation. In this paper, we mainly focus on the structure of parent storms.

2. 17 SEPTEMBER 2006 CASE OVERVIEW

Typhoon 0613 spawned three tornadoes in the Miyazaki Plain. Figure 1 shows the observed reflectivity field at 1400 JST (Japan Standard Time; UTC + 9 hours), when one of the tornadoes occurred. The center of T0613 (denoted by 'T' in Fig. 1) was 200 km west of the Kyushu Island. T0613 progressed northeastward and three tornadoes occurred in 300 km east-northeast from the center of T0613. Two distinct outer rainbands were found in the right-front quadrant of T0613 and well-developed convective cells within the outer rainbands moved north-northwestward. The tornado spawned at 1400 JST was accompanied by one of the well-developed cells (denoted by the open circle in Fig. 1). Other tornadoes were also generated by such developed cells. In the outer rainbands, the high equivalent potential temperature air was advected by the south-southeast flow in the lower troposphere and the low equivalent potential temperature air by the south-southwest flow in the middle troposphere. There was strong vertical wind shear below 2 km. The minima of pressure were observed just before the passes of all of the tornadoes and the wind direction changed temporally with the falling of pressure. Thus, the tornadoes were generated by the convective cells with mesocyclones, which progressed ahead of the tornadoes.

3. MODEL DESCRIPTION AND CONFIGURATION

The 5th generation of the Pennsylvania State University-National Center for Atmospheric Research Mesoscale

* *Corresponding author address:* Ken-ichi Shimose, University of Oklahoma, School of Meteorology, 120 David L. Boren Blvd., Rm 4119, Norman, OK 73072; e-mail: kshimose@ou.edu

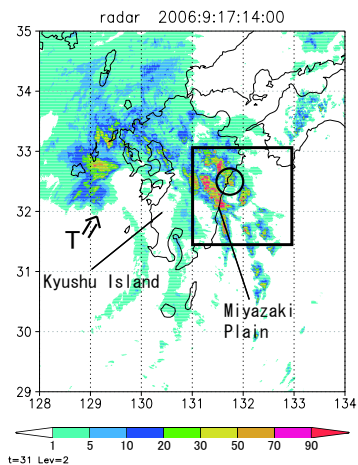


Figure 1: Radar reflectivity at 1400 JST. Unit of color bar is mm h^{-1} . 'T' indicates the center of T0613 and the arrow indicates the motion of T0613. The echo region marked by the open circle spawned the tornado. Open square is the region shown in Fig. 4

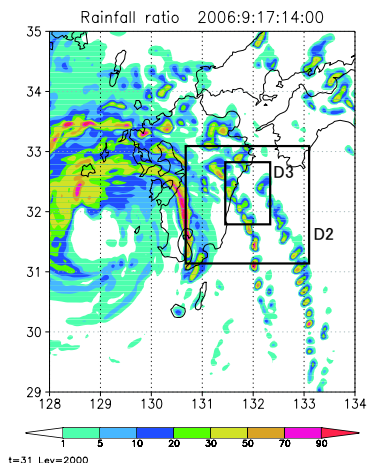


Figure 2: Simulated reflectivity at the level of 2 km at 1400 JST. Unit of color bar is mm h^{-1} . Black boundaries indicate boundaries of computational domains (D2: DOMAIN2, D3: DOMAIN3).

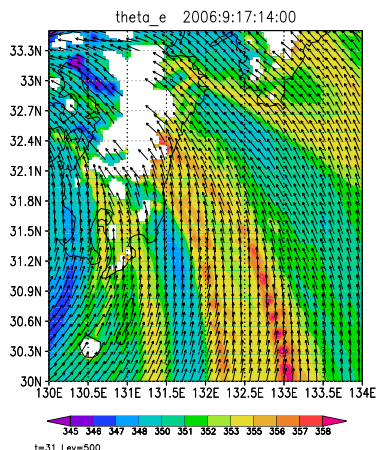


Figure 3: Simulated equivalent potential temperature and horizontal wind fields at the level of 0.5 km at 1400 JST.

Model (MM5) version 3.7, three-dimensional, compressible, nonhydrostatic model was used for the simulation. The explicit grid-scale microphysics followed the Goddard microphysics parameterization (Tao et al. 1993). This predicts fields of cloud water, rain water, snow, ice and graupel explicitly with microphysical processes. No cumulus parameterization was used in the simulation. The MRF PBL (Hong and Pan 1996) was employed for the planetary boundary layer. The model initial conditions and time-dependent lateral boundary conditions were derived from the objective analysis data, Regional-ANALysis (RANAL) produced by the Japan Meteorological Agency (JMA). These datasets assimilate the JMA spectral model analysis into the observational data. The resolution of these datasets is 20 km for the horizontal grid spacing and 21 levels in vertical. In the simulation presented here, three domains with 4 km, 0.9 km and 0.3 km resolution were used (Table 1, Fig. 2). DOMAIN 2 and 3 were two-way nesting and 35 half sigma levels from the surface to 100 hPa.

The simulation was started at 0900 JST 17 September 2006 and finished at 1800 JST. DOMAIN 2 started at 1100 JST and ended at 1500 JST in order to capture the storm scale fields. DOMAIN 3 was added from 1300 to 1430 JST to capture the low-level mesocyclone scale fields.

Table 1: Summary of the grid configuration used in the simulation.

	Grid points	Grid spacing	Vertical layers
DOMAIN 1	300×300	4.0 km	23
DOMAIN 2	301×301	0.9 km	35
DOMAIN 3	262×352	0.3 km	35
	Vertical grid:	Stretching grid	
	DOMAIN 2-3:	2-way nesting	

4. RESULTS

Typhoon 0613 as well as the outer rainbands is successfully simulated and the low-level mesocyclone and well-developed cells are captured. Figure 2 shows the simulated reflectivity field at the level of 2 km at 1400 JST. The distribution of the simulated reflectivity field is comparable to the observation field except for near the center of T0613. Two distinct outer rainbands with well-developed cells aligned like wave train are well simulated. Figure 3 shows the simulated equivalent potential temperature (θ_e) and horizontal wind fields at the level of 0.5 km at 1400 JST. Shear lines are found along

the outer rainbands. The high θ_e air is advected by the southeasterly flow and the areas of the high θ_e correspond to two outer rainbands.

Figure 4 shows the reflectivity field of DOMAIN 2 at the level of 2 km at 1340 JST, when the low-level vertical vorticity is most developed in this simulation. The simulated distribution of the reflectivity field corresponds to the observation field (denoted by the square in Fig. 1) and the echo region corresponding to the tornadic echo region in Fig. 1 exhibits the hook-shaped structure. Figure 5 shows the condensate mixing ratio and vertical vorticity fields of DOMAIN 3 at the level of 0.02 km at 1340 JST. There is the well-developed vertical vortex in the southeastern edge of the convective system. The value of the vertical vorticity exceeds 0.08 s^{-1} and the magnitude of the horizontal wind speed reaches 40 m s^{-1} . The simulated distribution of the condensate and vertical vorticity fields corresponds to the observed fields in the Great Plains (e.g., Dowell and Bluestein 2002; Alexander and Wurman 2004). Figure 6 shows the vertical vorticity and vertical velocity fields of DOMAIN 3 at the level of 2 km at 1340 JST. The vertical vorticity of the center of the system greatly exceeds 0.01 s^{-1} , the criterion for the mesocyclone (Doswell and Burgess 1993), and the updraft exceeds 10 m s^{-1} . The vertical cross section of the condensate mixing ratio and updraft fields along the solid line in Fig. 6 (Fig. 7) shows the deep convection, the high cloud top exceeding 10 km. Thus, the strong low-level mesocyclone is produced by the supercell storm. Some of simulated convective cells within the outer rainbands exhibit the same structure as above supercell.

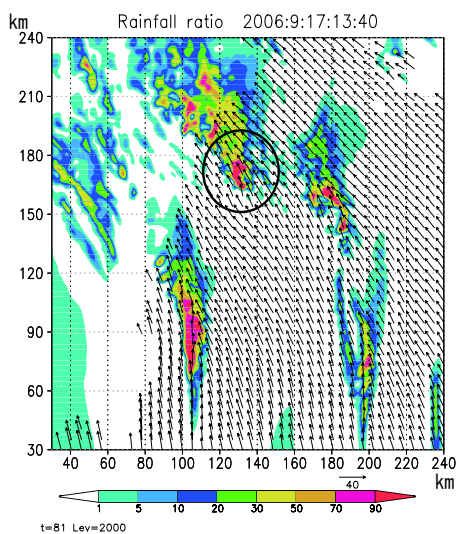


Figure 4: Simulated reflectivity ($z = 2 \text{ km}$) and horizontal wind ($z = 0.05 \text{ km}$) fields of DOMAIN 2 at the level at 1340 JST. Unit of color bar is mm h^{-1} . The circled echo exhibits the hook-shaped echo.

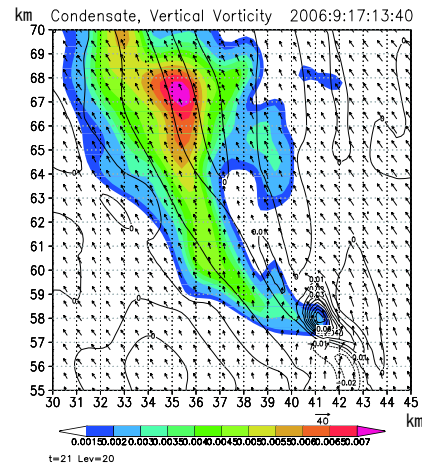


Figure 5: Simulated condensate mixing ratio and vertical vorticity fields of DOMAIN 3 at the level of 0.02 km at 1340 JST. Unit of color bar is kg kg^{-1} . Contour interval is 0.01 s^{-1} .

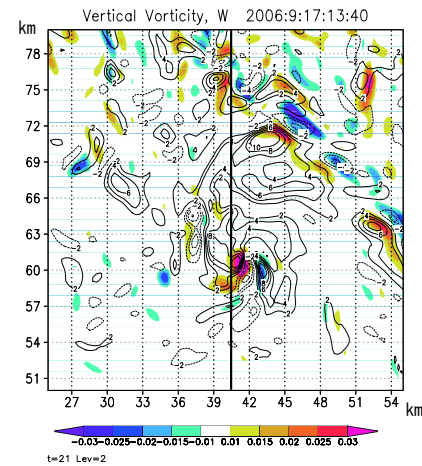


Figure 6: Simulated vertical vorticity and vertical velocity fields of DOMAIN 3 at the level of 2 km at 1340 JST. Unit of color bar is s^{-1} . Contour interval is 2 m s^{-1} . The vertical cross section along the black solid line is shown in Fig. 7.

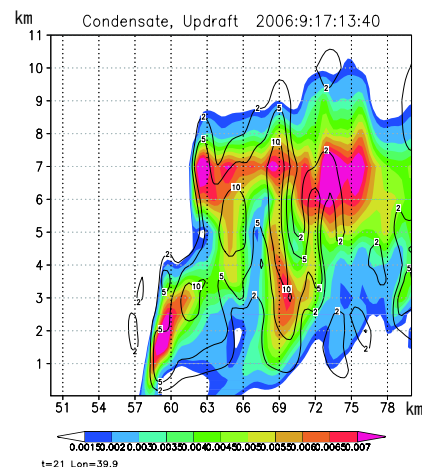


Figure 7: Vertical cross section of simulated condensate mixing ratio and updraft fields along the black solid line in Fig. 6. Unit of color bar is kg kg^{-1} . Contour interval is 2 m s^{-1} .

5. SUMMARY AND DISCUSSION

We simulate Typhoon 0613 which spawned three tornadoes in the outer rainbands and investigate the structure of convective cells and low-level mesocyclones within the outer rainbands. The convective cells within the outer rainbands are found along shear lines and high equivalent potential temperature air advected by the lower southeasterly flow. There is the strong mesocyclone ($\zeta \sim 0.08 \text{ s}^{-1}$) near the surface and the distribution of precipitation corresponds to the observed distribution in the Great Plains. The well-developed convective cell, which spawns the low-level mesocyclone, exhibits the hook-shaped echo and has the mesocyclone and strong updraft in its mid-level. Thus, the strong low-level mesocyclone is produced by the supercell storm. Some of the simulated convective cells within the outer rainbands exhibit the same structure as supercell mentioned above so that in this case, the tornadoes spawned in the Miyazaki Plain may be accompanied by supercell storms.

In past studies, the convective systems, within the tropical cyclones, spawned tornadoes exhibited shallow, small supercells so called as 'mini supercell' (e.g., McCaul and Weisman 1996; Spratt et al. 1997; Suzuki et al. 2000). In this case, however, the simulated supercell has the deep convection whose cloud top exceeds the height of 10 km. We need to investigate the difference of environment between the present case and past studies.

For future work, we attempt to perform 100 m resolution simulation to investigate the generation and development mechanism of the tornado itself.

Acknowledgements. Much of this work was done with support of JSPS Grant 18-9713. We are grateful to Dr. Hiroshi Niino who provided helpful advice. We also thank Dr. Michihiro Teshiba for his support.

REFERENCES

- Alexander, C. R., and J. Wurman, 2004: The 30 May 1998 Spencer, South Dakota, Storm. Part I: The structural evolution and environment of the tornadoes. *Mon. Wea. Rev.*, **133**, 72-96.
- Doswell, C. A. III, and D. W. Burgess, 1993: Tornadoes and tornadic storms: A review of conceptual models. *The Tornado: Its Structure, Dynamics, Prediction, and Hazards, Geophys. Monogr.*, No. 79, Amer. Geophys. Union, 161-172.
- Dowell, D. C., and H. B. Bluestein, 2002: The 8 June 1995 McLean, Texas, Storm. Part I: Observations of cyclic tornadogenesis. *Mon. Wea. Rev.*, **130**, 2626-2648.
- Gentry, R. C., 1983: Genesis of tornadoes associated with hurricanes. *Mon. Wea. Rev.*, **111**, 1793-1805.
- Hong, S.-Y., and H.-L. Pan, 1996: Nonlocal boundary layer vertical diffusion in a medium-range forecast model. *Mon. Wea. Rev.*, **124**, 2322-2339.
- McCaul, E. W., Jr., 1991: Buoyancy and shear characteristics of hurricane-tornado environments. *Mon. Wea. Rev.*, **119**, 1954-1978.
- , and M. L. Weisman, 1996: Simulations of shallow supercell storms in landfalling hurricane environments. *Mon. Wea. Rev.*, **124**, 408-429.
- Novlan, D. J., and W. M. Gray, 1974: Hurricane-spawned tornadoes. *Mon. Wea. Rev.*, **102**, 476-488.
- Saito, A., 1992: Mesoscale analysis of typhoon-associated tornado outbreaks in Kyushu Island on 13 October 1980. *J. Meteor. Soc. Japan*, **70**, 43-55.
- Spratt, S. M., D. W. Sharp, P. Welsh, A. Sandrik, F. Alsheimer, and C. Paxton, 1997: A WSR-88D assesment of tropical cyclone outer rainband tornadoes. *Wea. Forecasting*, **12**, 479-501.
- Suzuki, O., H. Niino, H. Ohno, and H. Nirasawa, 2000: Tornado-producing mini supercell associated with Typhoon 9019. *Mon. Wea. Rev.*, **128**, 1868-1882.
- Tao, W. K., and J. Simpson, 1993: Goddard Cumulus Ensemble Model. Part I: Model Description. *Terrestrial, Atmospheric and Oceanic Sciences*, **4**, 35-72.